Journal of Hepatocellular Carcinoma

Dovepress
Taylor & Francis Group

Open Access Full Text Article

ORIGINAL RESEARCH

Plasma Sphingolipid Profiling Predicts Radiosensitivity in Hepatocellular Carcinoma

Xiang Yuan[1,*], Kai Wang[2,*], Fengxin Chen[3], Xiurui Ge[1], Chen Xie[2], Yang Lei[2], Feng Lin[1], Yuqin Zhang[1], Yiyi Li[1]

[1]Department of Radiation Oncology, Nanfang Hospital, Southern Medical University, Guangzhou, Guangdong, People's Republic of China; [2]Hepatobiliopancreatic Surgery, Department of General Surgery, Nanfang Hospital, Southern Medical University, Guangzhou, Guangdong, People's Republic of China; [3]Department of Laboratory Medicine, Nanfang Hospital, Southern Medical University, Guangzhou, Guangdong, People's Republic of China

*These authors contributed equally to this work

Correspondence: Yiyi Li; Yuqin Zhang, Email liyiyi56@smu.edu.cn; 791369631@qq.com

Purpose: Radiotherapy constitutes a cornerstone in the management of hepatocellular carcinoma (HCC), but its efficacy is limited by radioresistance. Sphingolipids, a class of bioactive lipids, have been implicated in the metabolic reprogramming associated with treatment resistance. However, the potential of circulating sphingolipids as non-invasive biomarkers to predict radiosensitivity in HCC patients remains unexplored.

Patients and Methods: This prospective study enrolled 61 HCC patients scheduled for radiotherapy (NCT06864221). Pre-treatment plasma samples were analyzed via LC-MS/MS to quantify 13 sphingolipid species. The primary endpoint was objective response rate (ORR) per mRECIST at 12 weeks. Predictive models were developed using multivariate logistic regression with forward selection and LASSO, evaluated by AUC with bootstrap validation, calibration, and decision curve analysis. Longitudinal analysis was performed in a sub-cohort (n=25) with paired pre- and post-radiotherapy plasma samples.

Results: The objective response rate was 54.1%. Univariable analysis identified a distinct sphingolipid signature in responders, characterized by significantly lower S1P and higher levels of CER(d18:1/20:0) and CER(d18:1/24:1). These candidate biomarkers, along with significant clinical variables, were entered into multivariate modeling. The optimal integrated model (Model 1), selected via forward selection, comprised S1P, CER(d18:1/20:0), and the clinical factors ALP and TBIL, and excelled at predicting response (bootstrap-corrected AUC=0.930). A second model based on ceramide/S1P balance (CER(d18:1/26:1)/S1P, Total CER(d18:1)/S1P, AFP) also performed robustly (bootstrap-corrected AUC=0.828). Both models showed clinical utility per decision curve analysis. Longitudinal analysis revealed a coordinated metabolic shift in responders, with reduced S1P and elevated CER(d18:1/26:0), supporting a radiation-induced "sphingolipid rheostat" shift toward apoptosis.

Conclusion: This exploratory study provides the first clinical evidence that the baseline plasma sphingolipid profile is a potent, non-invasive predictor of HCC radiosensitivity, validating the "sphingolipid rheostat" theory. Our findings establish a framework for sphingolipid-guided precision radiotherapy and lay the necessary groundwork for future large-scale, multi-center validation trials, which hold significant potential to refine patient stratification and advance the development of novel metabolism-targeted interventions.

Plain Language Summary: Not all liver cancer patients benefit equally from radiotherapy, and doctors currently lack a good way to predict who will. Our study asked if a simple blood test could provide the answer by measuring specific fat molecules, called sphingolipids.

We analyzed blood from 61 patients before their radiotherapy. We discovered that distinct patterns of these sphingolipids could accurately identify who would respond well to the treatment. We even built two prediction models that showed excellent accuracy. Interestingly, in patients who did respond well, we saw a helpful shift in these molecules after treatment: protective signals decreased while those that encourage cancer cell death increased.

This means a straightforward blood test could one day help doctors personalize radiotherapy. By predicting a patient's response in advance, we can better match them with the most effective therapies. This approach could spare those unlikely to benefit from unnecessary side effects, while ensuring those who will respond get the maximum benefit—ultimately leading to more precise and effective cancer care for everyone.

https://doi.org/10.2147/JHC.S580242
Received: 9 November 2025
Accepted: 18 February 2026
Published: 25 February 2026

Keywords: biomarker, radiotherapy, predictive model, liquid chromatography-tandem mass spectrometry

Introduction

Hepatocellular carcinoma (HCC) is a leading cause of cancer mortality globally, with over 800,000 new cases and approximately 750,000 deaths annually, posing a major public health challenge.[1] Radiotherapy (RT) occupies a pivotal role in the therapeutic landscape of HCC, having evolved from a traditionally palliative modality to an indispensable cornerstone of multidisciplinary team (MDT) management. For patients deemed ineligible for surgical resection due to factors such as tumor location, inadequate hepatic functional reserve, or comorbidities, particularly those with portal vein tumor thrombosis (PVTT), RT—especially stereotactic body radiation therapy (SBRT)—has emerged as a crucial local treatment option with curative or neoadjuvant intent. Recent reviews consolidating clinical evidence indicate that SBRT can achieve local control rates exceeding 80% in HCC, underscoring its efficacy as a cornerstone of modern precision oncology.[2] Beyond providing effective local tumor control, RT plays versatile roles as conversion, bridging, and combination therapy within multidisciplinary management.[3] However, not all patients derive benefit from radiotherapy. Radioresistance remains a major clinical challenge limiting its broader application.[4] Metabolic reprogramming constitutes a key mechanism underpinning radioresistance development. This process involves alterations in glucose, lipid, amino acid, and other metabolic pathways, enabling tumor cells to rapidly adapt to the hypoxic, acidic, and nutrient-deprived tumor microenvironment (TME), thereby promoting their proliferation and conferring radioresistance.[5] Notably, sphingolipid metabolism intersects with these radioresistance mechanisms. Sphingolipids represent a class of bioactive lipid molecules with significant biological importance. Accumulating evidence from recent years demonstrates that sphingolipids are involved in regulating multiple critical cellular biological processes, including cell growth and survival, differentiation, angiogenesis, autophagy, and cell migration.[6] Importantly, research advances in the field of oncology over the past decade have firmly established sphingolipids as pivotal regulators of cell fate.[7]

The sphingolipid family encompasses key members such as ceramide (Cer), sphingosine (Sph), sphingosine-1-phosphate (S1P), ceramide-1-phosphate (C1P), sphingomyelin (SM), glucosylceramide (GlcCer), and gangliosides, among others. The liver serves as the primary site for sphingolipid metabolism. Research indicates that during the transformation of normal liver tissue into HCC tissue, metabolic reprogramming disrupts hepatic sphingolipid homeostasis. For instance, ceramide synthase 5 (CERS5), a key enzyme in the de novo biosynthesis of long-chain C16:0 ceramide, has been found to induce lipophagy. This process fuels cancer cell energy production, promotes membrane biosynthesis, and drives cellular proliferation.[8] Collectively, these findings underscore a close association between sphingolipid dysregulation and tumor biological behavior. Studies have demonstrated significant dysregulation of multiple sphingolipid metabolites in the plasma of patients with HCC.[9] Concurrently, additional research has identified specifically elevated levels of C16-ceramide and sphingosine-1-phosphate (S1P) in HCC patient plasma,[10] indicating that sphingolipid metabolic perturbations in HCC can be reflected by circulating biomarkers. Emerging evidence reveals a significant correlation between plasma sphingosine-1-phosphate (S1P) levels and immunotherapeutic response in HCC. Mechanistic investigations further demonstrate that plasma S1P is predominantly derived from secretory activities of tumor-associated macrophages (TAMs) within the tumor microenvironment.[11] Collectively, these findings suggest that plasma sphingolipid profiles may serve as non-invasive dynamic monitoring proxies for localized tumoral sphingolipid metabolic reprogramming, highlighting their substantial translational potential. Moreover, circulating sphingolipid levels have been validated to possess diagnostic and prognostic value across multiple malignancies, including pancreatic cancer,[12] prostate cancer,[13] gastric cancer,[14] breast cancer,[15] and colorectal cancer.[16] Critically, the intricate sphingolipid metabolic network serves as a pivotal regulator of intrinsic tumor radiosensitivity. Functionally, Radiotherapy induces apoptosis through multiple sphingolipid metabolic pathways, primarily by activating key enzymes including ceramide synthases (CERS), acid sphingomyelinase (ASMase), neutral sphingomyelinase (nSMase), sphingosine-1-phosphate lyase (SGPL1), and sphingosine-1-phosphate phosphatase (SGPP), while concurrently inhibiting sphingosine kinase-1 (SPHK1). Dysregulation of this metabolic axis—whether through insufficient post-RT activation or tumor-intrinsic reprogramming—compromises apoptotic efficacy and drives acquired resistance.[17] This balance is conceptualized as the "sphingolipid rheostat," where

the Cer/S1P ratio is pivotal in determining cellular responses to stress, including radiation.[18] Consequently, monitoring dynamic changes in plasma sphingolipids holds promise for predicting radiosensitivity in HCC.

To our knowledge, no study to date has investigated the clinical value of plasma sphingolipids as non-invasive biomarkers for predicting radiosensitivity in HCC patients. Given the interpatient heterogeneity in treatment response among HCC patients and the limitations of conventional predictors (eg, imaging and biopsy), including invasiveness and temporal latency, there is an urgent clinical need to develop non-invasive, precise biomarkers for guiding personalized treatment. In contrast to the limitations of conventional imaging-based or invasive predictors, plasma sphingolipid profiling offers a non-invasive, mechanism-informed approach that could potentially identify patients likely to respond to radiotherapy before or early during treatment. Against this backdrop, this exploratory pilot study aims to evaluate the potential of plasma sphingolipid profiles as predictors of HCC radiosensitivity. To address this gap, we conducted a pilot, exploratory study to investigate the potential association of plasma sphingolipids with radiotherapy response in a cohort of HCC patients. First, we sought to develop preliminary prediction models by integrating clinical features with sphingolipid profiles. Second, we explored the translational relevance of the "sphingolipid rheostat" theory by constructing models based on CER/S1P ratios to capture the balance between opposing signaling pathways. Finally, in a longitudinal sub-cohort, we employed multivariate analyses to visualize whether a consistent shift in the sphingolipid landscape was associated with treatment outcome. Collectively, this work aims to establish a methodological framework and provide preliminary evidence to inform the design of future, larger-scale studies on sphingolipid-guided precision radiotherapy in HCC.

Material and Methods

Patient Source and Enrollment Criteria

This study followed a single-center, prospective design for the development and preliminary validation of a predictive model. All participants were recruited from Nanfang Hospital, Southern Medical University, and each provided written informed consent.

The inclusion criteria were as follows: (i) age between 18 and 80 years; (ii) confirmed clinical or pathological diagnosis of primary liver cancer; (iii) an assessment by the attending physician that radiotherapy was indicated; and (iv) an expected survival period exceeding 3 months.

The exclusion criteria encompassed: (i) failure to complete radiotherapy or treatment interruption for any reason; (ii) presence of other primary malignant tumors; (iii) radiotherapy target volume located within the central nervous system (including the brain or spinal cord); (iv) uncontrolled underlying diseases that could potentially affect treatment outcomes or research results, such as hypertension (blood pressure >160/100 mmHg despite medication), diabetes (HbA1c >9%), or infections requiring intravenous antibiotics; (v) Severe metabolic diseases such as uncontrolled significant obesity, or fatty liver disease, which could significantly confound lipid metabolism analyses; (vi) failure to complete scheduled imaging evaluations within 3 months after radiotherapy; and (vii) receipt of local treatments (eg, interventional therapy or surgical resection) within 3 months after radiotherapy that could interfere with efficacy assessment.

This study was conducted in accordance with the Declaration of Helsinki and was approved by the Medical Ethics Committee of Nanfang Hospital (Approval No. NFEC-202407-K29) and registered on ClinicalTrials.gov (Registration No. NCT06864221), thereby ensuring standardized management throughout the entire process of study design and implementation.

Plasma Sample Collection and Sphingolipid Quantification

Whole blood samples were collected from all enrolled patients within 3 days before the initiation of radiotherapy and within 3 days after the completion of the entire radiotherapy course. All pre-radiotherapy blood draws were performed after a confirmed fasting period of at least 8 hours. Blood was drawn into EDTA-anticoagulant tubes, stored at 4°C, and centrifuged within 2 hours under the following conditions: 3500 rpm, room temperature, for 10 minutes. The resulting supernatant plasma was aliquoted and stored at −80°C in the hospital biobank.

Plasma Ceramide Extraction: Ceramides (CERs) were extracted using an ethyl acetate/isopropanol/water mixture (60/30/10, v/v/v). Buffer controls and pooled human plasma quality control (QC) samples were included. The internal standard CER

(d18:1/17:0) (Avanti Polar Lipids, Birmingham, AL, USA) was added during extraction. The extracts were dried under nitrogen stream and reconstituted in methanol. Quantitative analysis of the CER(d18:1) series was performed using liquid chromatography-tandem mass spectrometry (LC-MS/MS) on a Prelude SPLC+TSQ Quantiva system (Thermo Fisher Scientific, Waltham, MA, USA). A total of 10 CER(d18:1) species were detected: CER(d18:1/16:0), CER(d18:1/18:0), CER(d18:1/20:0), CER(d18:1/22:0), CER(d18:1/24:0), CER(d18:1/18:1), CER(d18:1/20:1), CER(d18:1/22:1), CER(d18:1/24:1), and CER(d18:1/26:1). Ceramide standards were purchased from Avanti Polar Lipids (Alabaster, AL, USA). Quantification was performed using a standard curve method, and concentrations were normalized to plasma volume.

Plasma Sphingosine and Sphingosine-1-phosphate Extraction: Sphingosine (SPH) and sphingosine-1-phosphate (S1P) were extracted from plasma using a methanol precipitation method. Buffer controls and pooled human plasma quality control (QC) samples were included. The internal standards C17-S1P (S1P(d17:1)) or C17-SPH (SPH(d17:1)) (Avanti Polar Lipids, Birmingham, AL, USA) were added during the extraction process. Briefly, 50 μL of thawed and homogenized plasma sample was aliquoted, followed by the addition of 10 μL of the corresponding internal standard working solution (2.5 mM in methanol) and 140 μL of methanol. The mixture was vortexed to precipitate proteins. Subsequently, the samples were centrifuged at 15,000 g for 20 minutes at room temperature. The supernatant was filtered through a nylon filter, transferred to an injection vial, and subjected to LC-MS/MS analysis.

HPLC-ESI-MS/MS Analysis of Sphingolipid Metabolites:[19] A 2 μL aliquot was injected into a Thermo SPLC system coupled to a triple quadrupole mass spectrometer. Chromatographic separation was achieved using an Agilent EclipsePlus C18 column. Mobile phase A consisted of methanol/water/formic acid (60:40:0.2, v/v/v), and mobile phase B was methanol/isopropanol/formic acid (60:40:0.2, v/v/v), both containing 10 mM ammonium acetate. The injection volume was 2 μL, the column temperature was maintained at 40°C, and the total run time was 22 minutes. The gradient program was as follows: 0–3 min, 0% to 10% B; 3–5 min, 10% to 40% B; 5–5.3 min, 40% to 55% B; 5.3–8 min, 55% to 60% B; 8–8.5 min, 60% to 80% B; 8.5–10.5 min, 80% B; 10.5–16 min, 80% to 90% B; 16–19 min, 90% B; 19–22 min, 90% to 100% B, at a flow rate of 0.4 mL/min, followed by a wash with 100% B and re-equilibration. ESI conditions were set in positive ion mode with the following parameters: nozzle voltage 300 V, capillary voltage 4000 V, nebulizer pressure 40 psi, drying gas flow 6 L/min, gas temperature 300°C, fragmentor voltage 150 V, skimmer voltage 65 V, and octopole RF peak 500 V. Collision energy (CE) was optimized between 20–60 eV. Data were processed using Thermo Scientific workstation software. Results were normalized to plasma volume.

Radiotherapy Treatment

Radiotherapy for liver cancer was delivered through a multidisciplinary team approach, including radiation oncologists, medical physicists, and radiation therapists. Treatment strategy was formulated based on comprehensive consideration of tumor diameter, number of lesions, proximity to critical organs (such as the intestines, spinal cord, and kidneys), liver function (Child-Pugh grade), and prior treatment history. The selection of specific radiotherapy techniques—such as 3-dimensional conformal radiotherapy (3D-CRT), intensity-modulated radiotherapy (IMRT), or stereotactic body radiotherapy (SBRT)—was determined by tumor morphology, vascular invasion, residual liver volume, and normal tissue tolerance doses. All treatment plans adhered to the recommendations of the International Commission on Radiation Units and Measurements (ICRU) Report No. 83 regarding target volume definition and dose specification, and clinical decision-making followed the National Comprehensive Cancer Network (NCCN) Clinical Practice Guidelines. Radiation doses were optimized using the biologically effective dose (BED) model, and fractionation schemes were dynamically adjusted on an individual basis based on normal tissue complication probability (NTCP) modeling.

Follow-Up and Study Endpoints

Baseline assessment was performed within 2 weeks before radiotherapy, including at least one imaging examination (contrast-enhanced computed tomography [CT] or magnetic resonance imaging [MRI]) and comprehensive recording of clinical information. Documented baseline data comprised: demographic characteristics (date of birth, sex); medical history (vital signs, height, weight, physical examination, time of diagnosis, prior history of surgery, radiotherapy, transarterial interventional therapy, and radiofrequency ablation); laboratory results (alpha-fetoprotein [AFP], bilirubin, alkaline phosphatase, alanine aminotransferase, aspartate aminotransferase, complete blood count, C-reactive protein,

procalcitonin, hepatitis B virus DNA load, etc).; and radiotherapy plan details (start and end dates of radiotherapy, treatment site, total dose, number of fractions, and technique).

The first follow-up was conducted at 12 weeks (±1 week) after radiotherapy completion and included serum AFP measurement, liver function tests, and at least one contrast-enhanced CT or MRI scan. Treatment response was evaluated according to the modified Response Evaluation Criteria in Solid Tumors (mRECIST), focusing on arterially enhancing lesions within the irradiated volume. Baseline tumor burden was quantified according to mRECIST criteria as the sum of the longest diameters (SLD) of the enhancing components for up to two target lesions per organ (with a maximum of five lesions in total). Responses were categorized as: complete response (CR): disappearance of any intratumoral arterial enhancement in all target lesions; partial response (PR): at least a 30% decrease in the sum of diameters of viable target lesions; stable disease (SD): any cases that do not qualify for either PR or progressive disease; progressive disease (PD): an increase of at least 20% in the sum of diameters of viable target lesions. To ensure an objective assessment, mRECIST evaluations were performed by radiologists blinded to the sphingolipid results, facilitated by strict data anonymization and access controls that separated the imaging review process from the biomarker data streams.

The primary endpoint of this exploratory study was the early radiographic objective response rate (ORR), defined as complete response (CR) + partial response (PR) according to mRECIST criteria assessed at 12 weeks post-radiotherapy. This endpoint was selected as it provides a direct measure of intrinsic tumor radiosensitivity, which is the central focus of this biomarker investigation.

Statistical Analysis

All statistical analyses were performed using R software (version 4.3.1). Continuous variables were presented as mean ± standard deviation or median (interquartile range), and categorical variables as frequency (percentage). Group comparisons between responders and non-responders were conducted using Student's *t*-test, Mann–Whitney *U*-test, Chi-squared test, or Fisher's exact test as appropriate. A two-sided p-value < 0.05 was considered statistically significant. As a prospective exploratory study investigating a novel biomarker hypothesis, no prior effect size was available for a formal sample size calculation. The cohort size was determined by clinical feasibility, representing consecutive eligible patients with complete data. To ensure robustness despite the sample size, we implemented rigorous internal validation and emphasize the preliminary, hypothesis-generating nature of the findings.

The analytical strategy comprised two primary workflows for predictive model development. First, an integrated clinical-sphingolipid model was constructed. In the univariable screening phase, to maximize sensitivity and avoid overlooking potentially important biomarkers, we analyzed all sphingolipid species and clinical variables without multiplicity adjustment, while acknowledging the associated risk of false positives, and subsequently incorporated variables significant at $p < 0.05$ into a multivariate logistic regression model with forward likelihood ratio selection to build the final model (Model 1). For all logistic regression models in this study, the outcome variable (radiotherapy response) was coded as 0 for responders and 1 for non-responders. Therefore, an odds ratio (OR) greater than 1 indicates a factor associated with a higher likelihood of non-response (radioresistance), whereas an OR less than 1 indicates a factor associated with a higher likelihood of response (radiosensitivity). Second, a model based on the ceramide/S1P balance was developed. To establish that the predictive value of these ratios extended beyond the effect of S1P alone, we performed two validation steps: 1) Spearman correlation analysis between each ratio and S1P levels, and 2) Analysis of covariance (ANCOVA) for each ratio variable, controlling for S1P concentration, with significance determined by a false discovery rate (FDR)-adjusted p-value < 0.1. Subsequently, to address multicollinearity among the ratio variables, least absolute shrinkage and selection operator (LASSO) regression with 10-fold cross-validation was employed for variable selection. To evaluate the incremental value of the sphingolipid ratios beyond a key clinical benchmark, alpha-fetoprotein (AFP) was added to the LASSO-selected variables in the final model (Model 2). The rationale for employing distinct variable selection methods was as follows: Forward selection was chosen for Model 1 to prioritize model parsimony and clinical interpretability when integrating a limited set of pre-filtered sphingolipid and clinical variables. In contrast, LASSO regression was adopted for Model 2 to handle the inherent multicollinearity among the multiple CER/S1P ratio variables and to perform automated variable selection from this correlated set.

Model performance was rigorously evaluated. Discriminatory ability was assessed by the area under the receiver operating characteristic curve (AUC). Calibration was evaluated using calibration plots. The clinical utility was quantified by decision curve analysis across a range of threshold probabilities. To estimate optimism and correct for overfitting, internal validation was performed using 1,000 bootstrap replicates. Model performance metrics, including accuracy, sensitivity, and specificity, were calculated across different classification thresholds.

For the longitudinal analysis of paired pre- and post-radiotherapy samples (n=25), unsupervised hierarchical clustering based on sphingolipid fold changes was performed. Partial least squares-discriminant analysis (PLS-DA) was used to identify sphingolipid species driving group separation, with variable importance in projection (VIP) scores calculated to rank metabolite contributions. Fold changes of key sphingolipids between responders and non-responders were compared using the [Mann–Whitney *U*-test] with FDR adjustment for multiple comparisons.

Results

Patient Characteristics and Treatment Response

This prospective study enrolled 61 consecutive patients with HCC treated with radiotherapy. Treatment response was assessed at 12 weeks (±1 week) after radiotherapy completion according to the modified Response Evaluation Criteria in Solid Tumors (mRECIST). A waterfall plot depicting the percentage change in the sum of target lesion diameters from baseline to the 12-week assessment timepoint illustrates the heterogeneity of treatment responses (Figure 1, individual values in Supplementary Table 1). The objective response rate (ORR) for the entire cohort was 54.1% (33/61), comprising 3 patients with a complete response (CR) and 30 with a partial response (PR). The non-responder group included 22 patients with stable disease (SD) and 6 with progressive disease (PD). Representative radiographic images for patients with responder and non-responder are presented in Figure 2, respectively. As summarized in Table 1, responders and non-responders exhibited significant differences in several key baseline characteristics, including AFP levels, Child-Pugh grade, total bilirubin (TBIL), and alkaline phosphatase (ALP) (all $p < 0.05$).

Association of Baseline Plasma Sphingolipids with Radiotherapy Outcome

We quantified a panel of 13 sphingolipids from pre-radiotherapy plasma samples in all 61 enrolled patients. The analyzed species included sphingosine (SPH), sphingosine-1-phosphate (S1P), and 11 ceramide (CER) isoforms: CER(d18:1/16:0), CER(d18:1/18:0), CER(d18:1/20:0), CER(d18:1/22:0), CER(d18:1/24:0), CER(d18:1/26:0), CER(d18:1/18:1), CER(d18:1/20:1), CER(d18:1/22:1), CER(d18:1/24:1), and CER(d18:1/26:1). Univariable analysis revealed significant disparities in the sphingolipid profiles between responders and non-responders. Figure 3 and Table 2 show that responders had significantly lower levels of S1P but higher levels of CER(d18:1/20:0) and CER(d18:1/24:1) compared to non-responders (all $p < 0.05$). The remaining ten sphingolipids did not demonstrate statistically significant differences between the two groups (see Table 2 for full details).

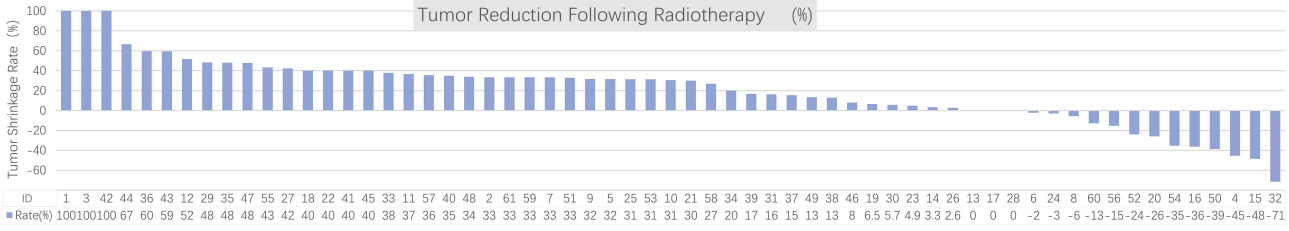

Figure 1 Waterfall plot of radiographic response in hepatocellular carcinoma patients following radiotherapy. The percentage change in the sum of target lesion diameters from baseline to the 12-week assessment timepoint is shown for each individual patient (n=61), as per mRECIST criteria. Patients are ranked from greatest tumor reduction (left) to greatest progression (right). The dotted horizontal lines demarcate the thresholds for partial response (PR, −30%) and progressive disease (PD, +20%). The objective response rate (ORR = CR + PR) for the cohort was 54.1%.

https://doi.org/10.2147/JHC.S580242

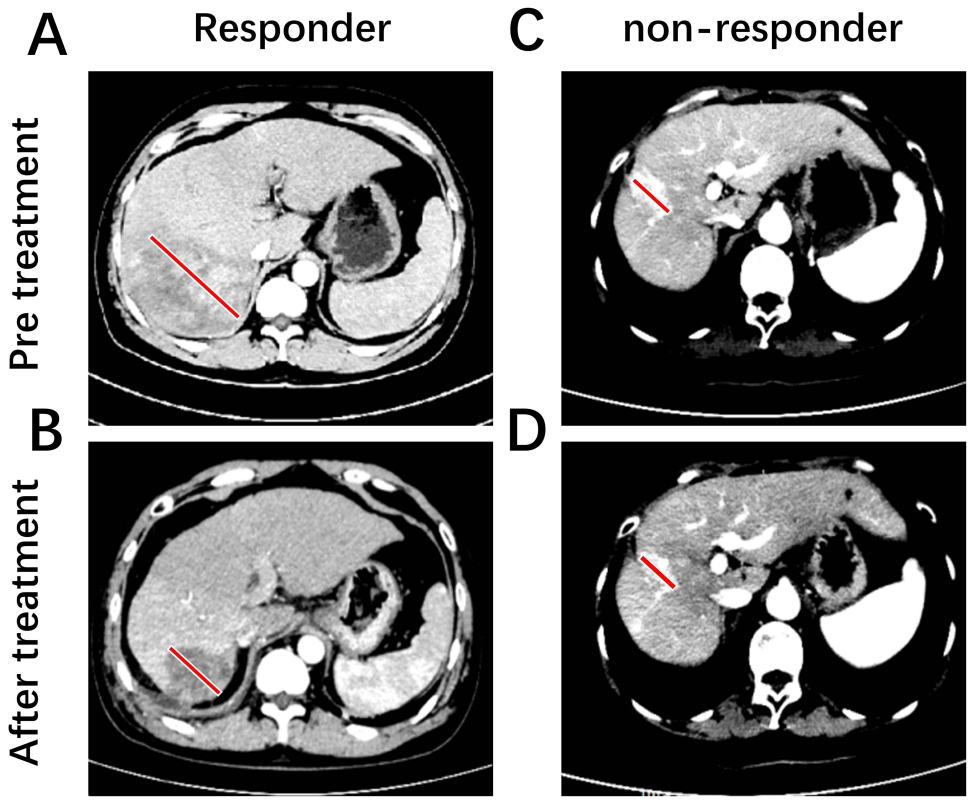

Figure 2 Representative contrast-enhanced CT images of hepatocellular carcinoma patients before and after radiotherapy, with tumor measurements per mRECIST criteria. (**A**) A patient from the responder group (ID-40): pre-radiotherapy arterial phase image shows an arterial hyperenhancing lesion, with the longest diameter measured by a solid line. (**B**) The same patient at the 12-week follow-up: arterial phase image shows a significant reduction in the longest diameter of the lesion (solid line), indicating a partial response. (**C**) A patient from the non-responder group (ID-13): pre-radiotherapy arterial phase image shows the target lesion with its longest diameter measured (solid line). (**D**) The same patient at the 12-week follow-up: arterial phase image shows persistent arterial enhancement with minimal change in the longest diameter (solid line), indicating stable disease.

Development of an Integrated Clinical-Sphingolipid Predictive Model

To systematically evaluate the predictive value of baseline plasma sphingolipids and clinical features for radiotherapy response in HCC, we implemented a sequential modeling strategy. First, we identified sphingolipid species significantly

Table 1 Baseline Characteristics of Hepatocellular Carcinoma Patients Stratified by Radiotherapy Response

Variables	Total (n = 61)	Responders (n = 33)	Non-responders (n = 28)	P value
Age(years)				
>60	15 (24.59%)	9 (27.27%)	6 (21.43%)	
≤60	46 (75.41%)	24 (72.73%)	22 (78.57%)	0.597
Gender				
Male	50 (81.97%)	29 (87.88%)	21 (75.00%)	
Female	11 (18.03%)	4 (12.12%)	7 (25.00%)	0.192
HbsAg				
+	46 (75.41%)	26 (78.79%)	20 (71.43%)	
-	15 (24.59%)	7 (21.21%)	8 (28.57%)	0.506
AFP (ng/mL)				
≥400	22 (36.07%)	7 (21.21%)	15 (53.57%)	
<400	39 (63.93%)	26 (78.79%)	13 (46.43%)	0.009**
Max Tumor size (cm)				
≤3	14 (22.95%)	9 (27.27%)	5 (17.86%)	
>3	47 (77.05%)	24 (72.73%)	23 (82.14%)	0.384

(*Continued*)

https://doi.org/10.2147/JHC.S580242

Table 1 (Continued).

Variables	Total (n = 61)	Responders (n = 33)	Non-responders (n = 28)	P value
Child Pugh grade				
A	41 (67.21%)	27 (81.82%)	14 (50.00%)	
B	20 (32.79%)	6 (18.18%)	14 (50.00%)	0.008**
BCLC stage				
A	10 (16.39%)	4 (12.12%)	6 (21.43%)	
B	4 (6.56%)	3 (9.09%)	1 (3.57%)	
C	47 (77.05%)	26 (78.79%)	21 (75.00%)	0.465
Lesions with prior intervention				
Yes	45 (73.77%)	24 (72.73%)	21 (75.00%)	
No	16 (26.23%)	9 (27.27%)	7 (25.00%)	0.841
ALBI score				
1	21 (34.43%)	11 (33.33%)	10 (35.71%)	
2	39 (63.93%)	22 (66.67%)	17 (60.71%)	
3	1 (1.64%)	0	1 (3.58%)	0.525
Prior targeted/immuno-therapy				
Yes	37 (60.66%)	22 (66.67%)	15 (53.57%)	
No	24 (39.34%)	11 (33.33%)	13 (46.43%)	0.297
ALT (U/L)				
≤40	38 (62.30%)	19 (57.58%)	19 (67.86%)	
>40	23 (37.70%)	14 (42.42%)	9 (32.14%)	0.409
AST (U/L)				
≤40	26 (42.62%)	15 (45.45%)	11 (39.29%)	
>40	35 (57.38%)	18 (54.55%)	17 (60.71%)	0.627
TBIL (μmol/L)				
≤17.1	49 (80.33%)	30 (90.91%)	19 (67.86%)	
>17.1	12 (19.67%)	3 (9.09%)	9 (32.14%)	0.024*
ALB (g/L)				
≤35	24 (39.34%)	11 (33.33%)	13 (46.43%)	
>35	37 (60.66%)	22 (66.67%)	15 (53.57%)	0.297
ALP (U/L)				
≤150	39 (63.93%)	25 (75.76%)	14 (50.00%)	
>150	22 (36.07%)	8 (24.24%)	14 (50.00%)	0.037*
WBC (x10^9)	5.68 (3.76;7,60)	5.98 (4.36;7.60)	5.32 (3.13;7.51)	0.179
LYM (x10^9)	1.35 (0.57;2,13)	1.41 (0.70;2.12)	1.28 (0.38;2.18)	0.548
NEU (x10^9)	3.73 (2.09;5.37)	3.86 (2.38;5.34)	3.57 (1.75;5.39)	0.490
MONO (x10^9)	0.56 (0.30;0.82)	0.60 (0.33;0.87)	0.51 (0.26;0.76)	0.191
HB (g/L)	124 (85;163)	126 (86;166)	123 (87;159)	0.529
PLT (x10^9)	163 (80;246)	175 (94;256)	149 (63;235)	0.239
Radiation Target Sites				
Primary	51 (83.61%)	27 (81.82%)	24 (85.71%)	0.682
Metastases	10 (16.39%)	6 (18.18%)	4 (14.29%)	
BED (Gy)				
<80	40 (65.57%)	22 (66.67%)	18 (64.29%)	
≥80	21 (34.43%)	11 (33.33%)	10 (35.71%)	0.845
Fractionation Schedule				
Hypofractionated	17 (27.87%)	11 (33.33%)	6 (21.43%)	
Conventional	44 (72.13%)	22 (66.67%)	22 (78.57%)	0.301
Hypertension				
Yes	11 (18.03%)	8 (24.24%)	3 (10.71%)	
No	50 (81.87%)	25 (75.76%)	25 (89.29%)	0.171

(*Continued*)

Table 1 (Continued).

Variables	Total (n = 61)	Responders (n = 33)	Non-responders (n = 28)	P value
Diabetes mellitus				
Yes	10 (16.39%)	5 (15.15%)	5 (17.86%)	
No	51 (83.61%)	28 (84.85%)	23 (82.14%)	0.522
BMI (kg/m^2)	23.1 (19.4;26,8)	23.2 (18.8;27.6)	23.1 (20.0;26.2)	0.935
PIV	347 (118;576)	366 (123;609)	325 (116;534)	0.781
SII	545 (130;960)	562 (199;925)	525 (129;921)	0.732

Notes: Data are presented as n (%) or median (interquartile range). Group comparisons were performed using the Chi-squared test, Fisher's exact test, Student's *t*-test, or Mann–Whitney *U*-test, as appropriate (* p < 0.05, ** p < 0.01).

associated with treatment response in univariable analysis from a panel of 13 metabolites, establishing them as candidate biomarkers within this metabolic axis (S1P, CER(d18:1/20:0), CER(d18:1/24:1)). These candidate sphingolipids were then combined with four clinical variables significant in univariable analysis (Child-Pugh score, AFP, ALP, TBIL) and incorporated into a multivariate logistic regression model using forward likelihood ratio selection. This approach aimed to construct an integrated model to assess the independent and combined predictive value of the sphingolipid metabolic network within a clinical context.

The optimal integrated model (hereinafter referred to as the model 1) comprised S1P, CER(d18:1/20:0), and the clinical variables ALP and TBIL. Detailed parameters of this final model are presented in Table 3. Within the model, S1P

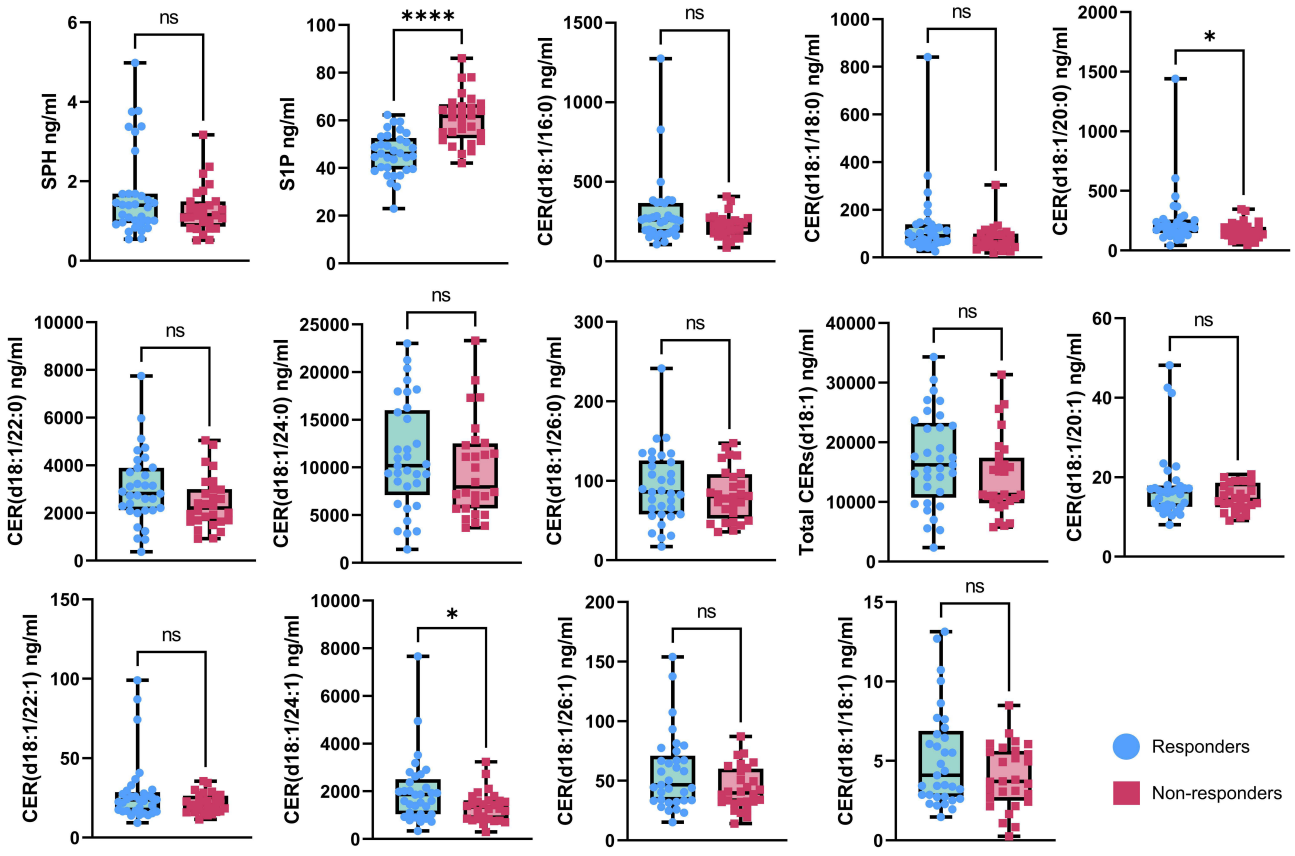

Figure 3 Baseline plasma sphingolipid profiles differ between radiotherapy responders and non-responders. Concentrations of sphingosine (SPH), sphingosine-1-phosphate (S1P), and 11 ceramide (CER) isoforms were quantified in the plasma of hepatocellular carcinoma patients scheduled for radiotherapy using targeted lipidomics. The analyzed ceramide species were CER(d18:1/16:0), CER(d18:1/18:0), CER(d18:1/20:0), CER(d18:1/22:0), CER(d18:1/24:0), CER(d18:1/26:0), CER(d18:1/18:1), CER(d18:1/20:1), CER(d18:1/22:1), CER (d18:1/24:1), CER(d18:1/26:1) and total CER(d18:1). Data are presented using box plots. Blue circles represent responders; red squares represent non-responders. Center lines in the box plots show the medians; box limits indicate the upper and lower quartiles; ****p < 0.0001; *p < 0.05; ns, not significant (Mann–Whitney *U*-test).

https://doi.org/10.2147/JHC.S580242

Table 2 Baseline Plasma Sphingolipid Profiles of Hepatocellular Carcinoma Patients Stratified by Radiotherapy Response

Plasma Sphingolipids	Total (n = 61)	Responders (n = 33)	Non-responders (n = 28)	P value
SPH	1.29(0.95;1.68)	1.40(0.95;1.69)	1.16(0.86;1.49)	0.336
S1P	51.74(44.54;61.68)	46.05(39.41;52.58)	61.68(52.47;66.76)	8.61E-07***
CER(d18:1/16:0)	241.71(175.71;279.18)	260.13(180.75;366.71)	218.46(166.36;264.12)	0.118
CER(d18:1/18:0)	76.37(54.38;116.35)	90.23(60.50;138.78)	70.67(44.54;99.61)	0.052
CER(d18:1/20:0)	182.11(129.76;234.62)	198.74(146.50;259.13)	153.94(102.48;197.65)	0.024*
CER(d18:1/22:0)	2594.52(1885.16;3453.50)	2814.10(2111.29;3893.93)	2202.65(1651.81;2996.10)	0.062
CER(d18:1/24:0)	9681.81(6072.12;13485.3)	10185.33(7092.70;16015.27)	7945.89(5687.55;12517.99)	0.339
CER(d18:1/26:0)	82.87(57.71;114.41)	85.89(57.71;125.52)	80.24(52.39;108.46)	0.524
CER(d18:1/18:1)	3.72(2.71;6.06)	4.09(2.74;6.88)	3.71(2.50;5.62)	0.265
CER(d18:1/20:1)	15.45(12.48;17.90	16.32(12.54;17.90)	14.37(12.40;18.57)	0.385
CER(d18:1/22:1)	22.34(16.52;27.24)	23.79(16.69;28.67)	20.84(16.24;26.43)	0.311
CER(d18:1/24:1)	1457.08(915.40;2002.79)	1858.45(1040.49;2504.78)	1327.27(835.90;1617.22)	0.029*
CER(d18:1/26:1)	43.35(32.55;65.00)	46.62(33.35;71.07)	39.82(32.31;60.03)	0.108
Total CERs(d18:1)	15113.38(9983.11;20818.08)	16215.92(10730.05;23243.70)	11247.37(9770.73;17406.14)	0.144

Notes: Plasma sphingolipid concentrations are presented as median (interquartile range) in ng/mL. Statistical significance between responders and non-responders was determined using the Mann–Whitney *U*-test (* $p < 0.05$, *** $p < 0.001$).

Table 3 Multivariable Logistic Regression Analysis of the Integrated Clinical-Sphingolipid Model for Predicting Radiotherapy Response

Variable	Beta	Odds Ratio (OR)	95% CI	p-value
S1P	0.271	1.312	1.157–1.595	0.0006
CER(d18:1/20:0)	−0.016	0.984	0.969–0.995	0.0168
ALP (high vs low)	1.64	5.156	0.986–35.197	0.0658
TBIL (high vs low)	1.558	4.751	0.699–44.346	0.1291
(Intercept)	−12.583	0	0-0.002	0.0009

Notes: This table presents the final multivariate logistic regression model (Model 1) derived from forward selection, integrating significant clinical and sphingolipid variables. The outcome was coded as 1 for non-response and 0 for response. Therefore, an OR > 1 indicates a factor associated with a higher likelihood of non-response (radioresistance), while an OR < 1 indicates a factor associated with a higher likelihood of response (radiosensitivity). The "high vs low" groups for ALP and TBIL were defined according to the thresholds specified in Table 1.

was an independent risk factor (OR = 1.312, 95% CI: 1.157–1.595), whereas CER(d18:1/20:0) was an independent protective factor (OR = 0.984, 95% CI: 0.969–0.995). The integrated model demonstrated exceptional discriminative ability in the training set, achieving an area under the curve (AUC) of 0.943. Model comparison revealed that its performance was numerically superior to all individual predictors, and its AUC exceeded those of both the Sphingolipids-Only Model (AUC: 0.924) and the Clinical-Only Model (AUC: 0.712) (Figure 4; detailed model parameters in Supplementary Table 2).

To evaluate the robustness and generalizability of the integrated model, we performed 1000 bootstrap internal validation replicates. The results yielded a corrected AUC of 0.930 (95% CI: 0.886–0.947) with an optimism of only 0.013, indicating a minimal risk of overfitting and excellent internal validity (Figure 5A). The calibration curve showed good agreement between predicted probabilities and observed event rates across all risk strata, further affirming the model's accuracy (Figure 5B; calibration data in Supplementary Table 3).

To further assess its potential for clinical translation, we generated a decision curve analysis (DCA). Across the majority of threshold probabilities (approximately 1% to 80%), the use of the integrated model for clinical decision-making provided a net benefit that was substantially higher than the "treat all" or "treat none" strategies, and was also superior to the net benefit offered by either the Sphingolipids-Only or Clinical-Only models (Figure 5C; decision curve data in Supplementary Table 4). This suggests that employing the integrated model can yield greater clinical net benefit.

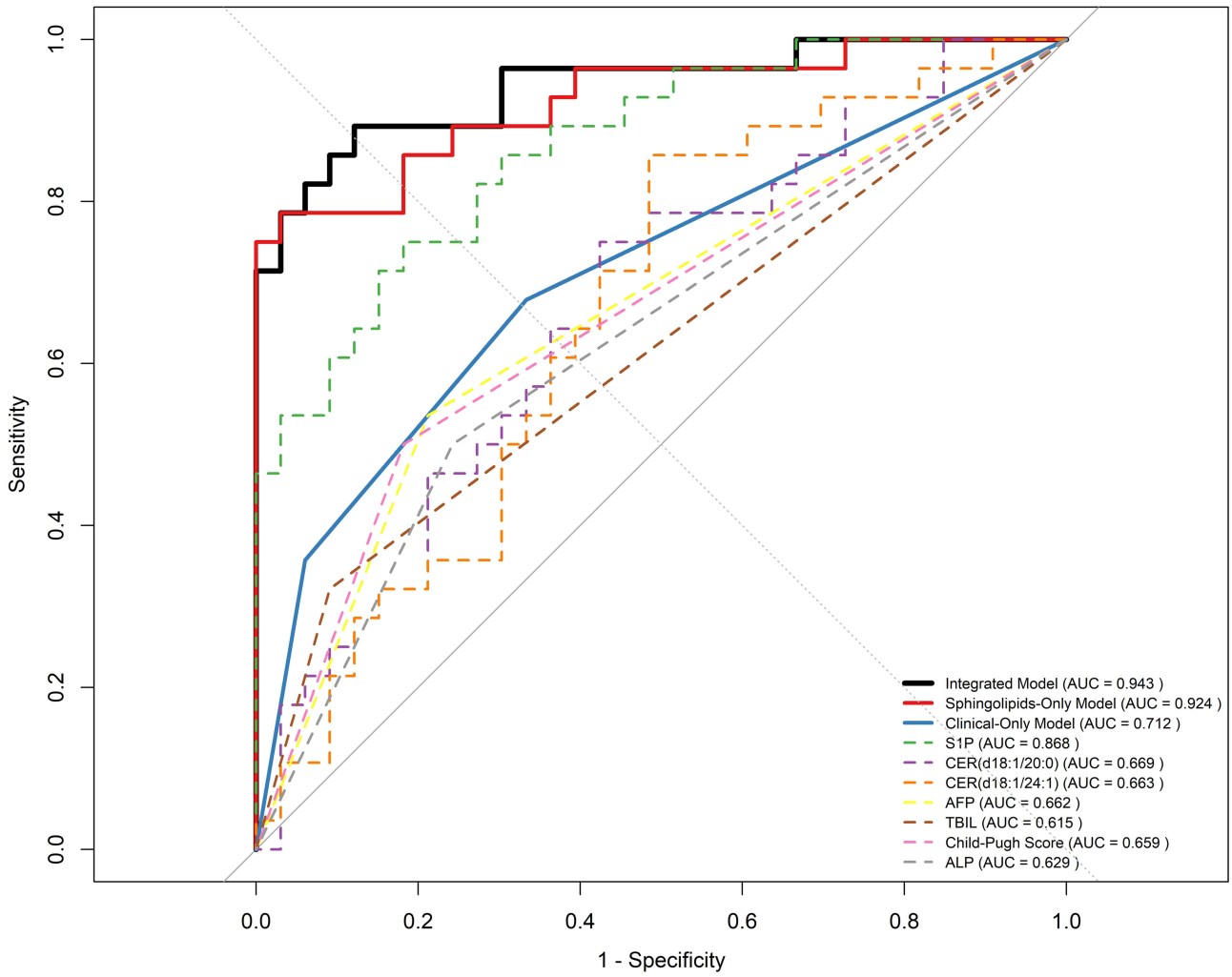

Figure 4 Receiver operating characteristic (ROC) curves for predicting radiotherapy response. The performance of the integrated clinical-sphingolipid model (Model 1, black solid line) is compared against its individual components (S1P, CER(d18:1/20:0), ALP, TBIL), the Sphingolipids-Only model (red dashed line), and the Clinical-Only model (blue dotted line). The integrated model (AUC=0.943) demonstrates superior discriminatory ability. The diagonal grey line represents a classifier with no discriminative ability (AUC=0.5).

Additionally, we evaluated the performance of the integrated model across different classification thresholds (Figure 5D; full performance metrics in Supplementary Table 5). Using the maximization of the F1-score (the harmonic mean of precision and recall) as the criterion, a threshold of 0.5 was identified as optimal. At this threshold, the model achieved an accuracy of 88.5%, with sensitivity and specificity of 89.3% and 87.9%, respectively, representing the best balance. To accommodate different clinical objectives: the threshold can be lowered to 0.2 to maximize sensitivity (96.4%) for scenarios aiming to identify all potential responders; conversely, it can be raised to 0.8 to maximize specificity (100%) for scenarios prioritizing the selection of patients with a very high probability of response.

A Predictive Model Based on the Ceramide/S1P Ratio for Radiotherapy Response

To further investigate the predictive value of sphingolipid metabolic balance beyond individual molecules, we calculated the ratios of 12 ceramide species to S1P. Univariable analysis revealed that all ratio variables were significantly different between responders and non-responders (all FDR-adjusted $P < 0.05$; Figure 6 and Supplementary Table 6). To confirm that the predictive value of these ratios was not merely a reflection of S1P effects, we performed systematic validation. First, Spearman correlation analysis (Supplementary Figure 1) showed that these ratios were only weakly to moderately negatively correlated with S1P levels (r^s range: −0.13 to −0.64), indicating they carry independent information. More

https://doi.org/10.2147/JHC.S580242

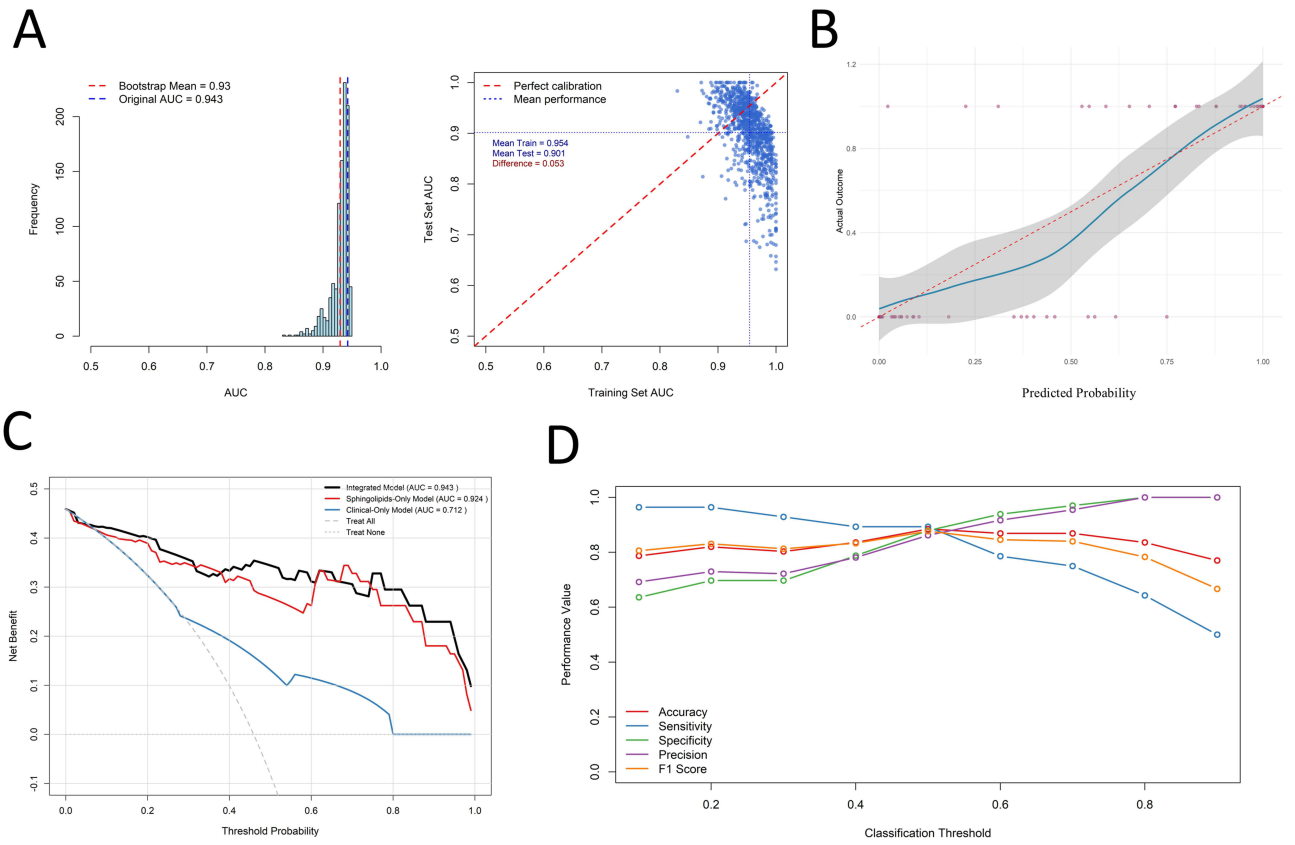

Figure 5 Internal validation and clinical utility of the integrated clinical-sphingolipid model (Model 1). (**A**) Bootstrap-validated ROC curve after 1000 replicates (corrected AUC=0.930). (**B**) Calibration curve showing the agreement between the predicted probability of response and the observed fraction of patients with response. The dotted diagonal line represents perfect calibration. (**C**) Decision curve analysis (DCA) showing the net benefit of using Model 1 for clinical decision-making across a range of threshold probabilities, compared to the "treat all" and "treat none" strategies, as well as the Sphingolipids-Only and Clinical-Only models. (**D**) Model performance metrics (Accuracy, Sensitivity, Specificity) across different classification thresholds. The highest balance between precision and recall (F1-score = 0.877) was achieved at a threshold of 0.5.

critically, in an analysis of covariance (ANCOVA) controlling for S1P levels (Supplementary Table 7), six ratio variables remained significant after FDR adjustment (FDR < 0.1), including: CER(d18:1/22:0)/S1P, CER(d18:1/24:0)/S1P, CER (d18:1/26:0)/S1P, CER(d18:1/18:1)/S1P, CER(d18:1/26:1)/S1P, and Total CER(d18:1)/S1P. This result provides strong evidence that the predictive effect of these specific CER/S1P balance relationships on radiotherapy response is independent of the absolute concentration of S1P.

Based on the foregoing analysis, we selected these six independent ratio variables, along with the four clinical variables significant in univariable analysis (Child-Pugh score, AFP, ALP, TBIL), for the model construction pipeline. Given the severe multicollinearity among these ratio variables, we employed LASSO regression for variable selection. After determining the optimal penalty parameter (λ) via 10-fold cross-validation, the LASSO regression selected the two sphingolipid ratio variables with the strongest predictive power: CER(d18:1/26:1)/S1P and Total CER(d18:1)/S1P (Figure 7A; Coefficient Path in Supplementary Figure 2; final LASSO selection in Supplementary Table 8). Although LASSO regression did not select any clinical variables, alpha-fetoprotein (AFP) was retained in the final model due to its established prognostic value in HCC, allowing us to assess the incremental predictive contribution of the sphingolipid ratios above and beyond this key clinical benchmark.

This resulted in a logistic regression model comprising CER(d18:1/26:1)/S1P, Total CER(d18:1)/S1P, and AFP (hereinafter referred to as the model 2). Detailed parameters of this model are presented in Table 4. Within the model, both sphingolipid ratios were protective factors, with an odds ratio (OR) of 0.142 (95% CI: 0.017–0.779) for CER(d18:1/26:1)/S1P and an OR of 0.995 (95% CI: 0.989–1.000) for Total CER(d18:1)/S1P. Conversely, AFP was a risk factor, with

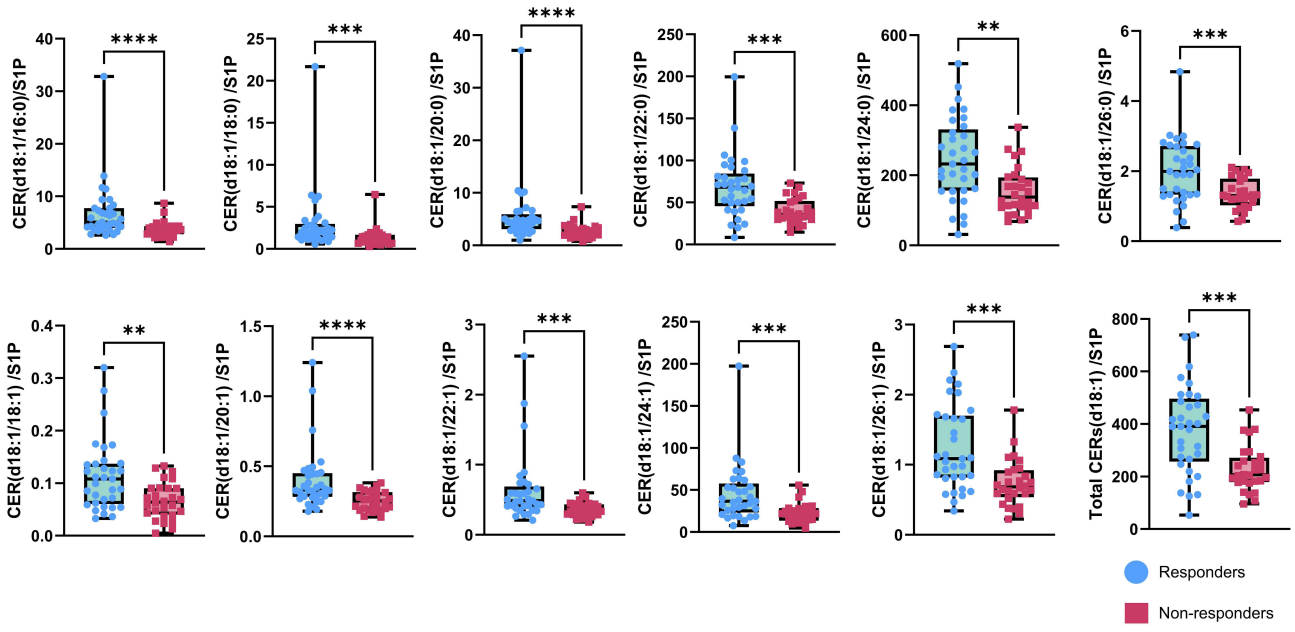

Figure 6 Baseline plasma CER/S1P ratio profiles differ between radiotherapy responders and non-responders. Comparison of the ratio of multiple ceramide species to Sphingosine-1-phosphate (S1P) between radiotherapy responders (n=33) and non-responders (n=28). The analyzed ceramide species were CER(d18:1/16:0)/S1P, CER(d18:1/18:0) /S1P, CER(d18:1/20:0) /S1P, CER(d18:1/22:0) /S1P, CER(d18:1/24:0) /S1P, CER(d18:1/26:0) /S1P, CER(d18:1/18:1) /S1P, CER(d18:1/20:1) /S1P, CER(d18:1/22:1) /S1P, CER(d18:1/24:1) /S1P, CER(d18:1/26:1) /S1P and total CER(d18:1) /S1P. Data are presented using box plots. Blue circles represent responders; red squares represent non-responders. Center lines in the box plots show the medians; box limits indicate the upper and lower quartiles; ****$p < 0.0001$; ***$p < 0.001$; **$p < 0.01$ (Mann–Whitney *U*-test).

an OR of 5.372 (95% CI: 1.402–25.220). The ratio model demonstrated good discriminative ability in the training set, with an area under the curve (AUC) of 0.839, performing significantly better than any single predictor (Figure 7B).

To assess the model's robustness, we performed 1000 bootstrap internal validation replicates. The results showed a corrected AUC of 0.828 (95% CI: 0.798–0.845) and a low optimism of 0.010, indicating a minimal risk of overfitting (Figure 7C). The calibration curve showed good agreement between the predicted probabilities and the observed event rates (Figure 7D; calibration data in Supplementary Table 9). Decision curve analysis demonstrated that across the majority of threshold probabilities (approximately 1% to 70%), the use of this ratio model for decision-making provided a net benefit that was substantially higher than the "treat all" or "treat none" strategies, and was also superior to the net benefit offered by relying on AFP or the sphingolipid ratios alone (Figure 7E; decision curve data in Supplementary Table 10).

Additionally, we evaluated the model's performance across different classification thresholds (Figure 7F; full performance metrics in Supplementary Table 11). Using the maximization of the F1-score as the criterion, a threshold of 0.3 was identified as optimal. At this threshold, the model maintained high sensitivity (85.7%) while achieving good specificity (75.8%), with an accuracy of 80.3% and an F1-score of 0.818, representing the best diagnostic balance.

Dynamic Remodeling of the Sphingolipid Network Following Radiotherapy

To investigate the dynamic effects of radiotherapy on the plasma sphingolipid metabolic network, we performed a longitudinal lipidomic analysis on all patients from the main cohort (n=61) from whom paired pre- and post-radiotherapy plasma samples were available (n=25). This subset included 17 responders and 8 non-responders. Unsupervised hierarchical clustering analysis, based on the profiles of sphingolipid fold changes, segregated the patients into two primary clusters (Figure 8A; heatmap data in Supplementary Table 12). This data-driven clustering demonstrated a statistically significant association with clinical response status ($p < 0.01$, Fisher's exact test). One cluster was significantly enriched with non-responders (7/11, 63.6%), whereas the other consisted almost entirely of responders (13/14, 92.9%).

To pinpoint the specific sphingolipid species driving this separation, we performed partial least squares-discriminant analysis (PLS-DA). The PLS-DA score plot revealed a clear separation between responders and non-responders in the metabolic space (Figure 8B; PLS-DA score data in Supplementary Table 13), indicating divergent dynamic remodeling

https://doi.org/10.2147/JHC.S580242

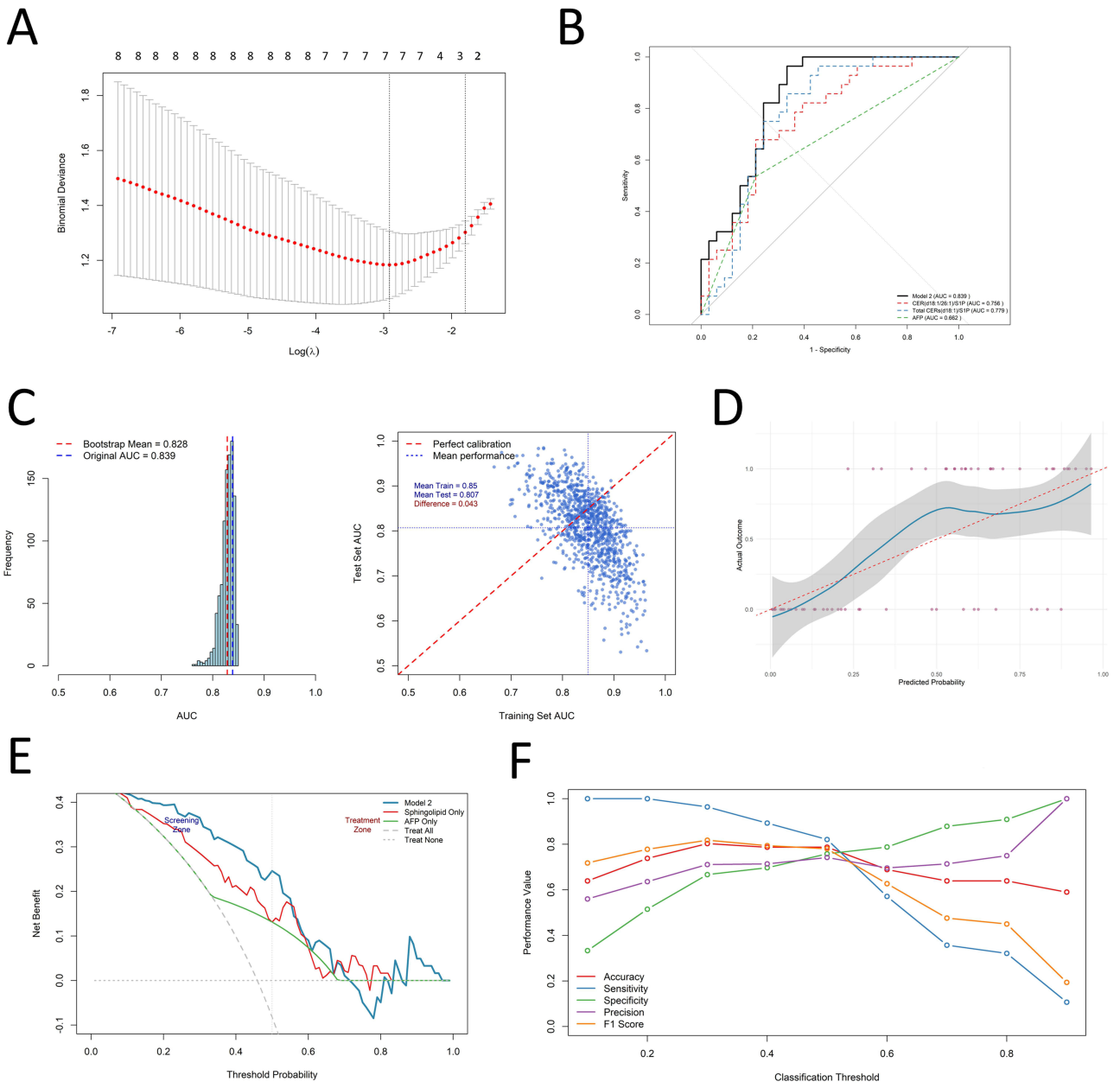

Figure 7 Development and validation of the ceramide/S1P ratio-based predictive model (Model 2). (**A**) LASSO coefficient profiles of the six candidate ceramide/S1P ratio variables. A vertical line is drawn at the value chosen by 10-fold cross-validation (optimal λ), where the two most predictive variables (CER(d18:1/26:1)/S1P and Total CER (d18:1)/S1P) were retained. (**B**) ROC curve of the final ratio-based model (Model 2, AUC=0.839). (**C**) Bootstrap-validated ROC curve (corrected AUC=0.828). (**D**) Calibration curve for Model 2. (**E**) Decision curve analysis (DCA) showing the net benefit of using Model 2 for clinical decision-making across a range of threshold probabilities, compared to the "treat all" and "treat none" strategies, as well as the Sphingolipids-Only and AFP-Only models. (**F**) Model performance metrics across different classification thresholds for Model 2. The highest balance between precision and recall (F1-score = 0.818) was achieved at a threshold of 0.3.

of their sphingolipid metabolomes following radiotherapy. Variable Importance in Projection (VIP) analysis identified six sphingolipid species as the primary drivers of this group separation (VIP > 1.0) (Figure 8C; VIP scores data in Supplementary Table 14). Ceramide species CER(d18:1/26:0) (VIP = 1.458), sphingosine (SPH, VIP = 1.409), and sphingosine-1-phosphate (S1P, VIP = 1.376) were the top contributors, followed by CER(d18:1/24:0), Total CER(d18:1), and CER(d18:1/22:0).

We next quantitatively compared the post-radiotherapy fold changes (Log2FC) of these key sphingolipids between the two groups. Although the between-group differences for some species were attenuated after stringent multiple comparison correction, their dynamic changes exhibited a highly coordinated and consistent pattern. Specifically, among the six highest-

Table 4 Multivariable Logistic Regression Analysis of the Ceramide/S1P Ratio-Based Model for Predicting Radiotherapy Response

Variable	Beta	Odds Ratio (OR)	95% CI	p-value
CER(d18:1/26:1)/S1P	−1.951	0.142	0.017–0.779	0.041
Total CERs(d18:1)/S1P	−0.005	0.995	0.989–1	0.0876
AFP (high vs low)	1.681	5.372	1.402–25.22	0.0202
(Intercept)	2.541	12.688	2.302–94.528	0.0065

Notes: This table presents the final multivariate logistic regression model (Model 2) based on the ceramide/S1P balance concept, incorporating variables selected by LASSO regression and the clinically established biomarker AFP. The outcome was coded as 1 for non-response and 0 for response. Therefore, an OR > 1 indicates a factor associated with a higher likelihood of non-response (radioresistance), while an OR < 1 indicates a factor associated with a higher likelihood of response (radiosensitivity). The "high vs low" group for AFP was defined as ≥400 ng/mL vs <400 ng/mL, as specified in Table 1.

VIP species, the pro-apoptotic ceramide CER(d18:1/26:0) exhibited a significantly greater increase in responders compared to non-responders (FDR-adjusted P = 0.011), while the pro-survival lipid S1P was significantly decreased in responders (FDR-adjusted P = 0.047). Most importantly, the direction of change for all VIP sphingolipids aligned perfectly with the predictions

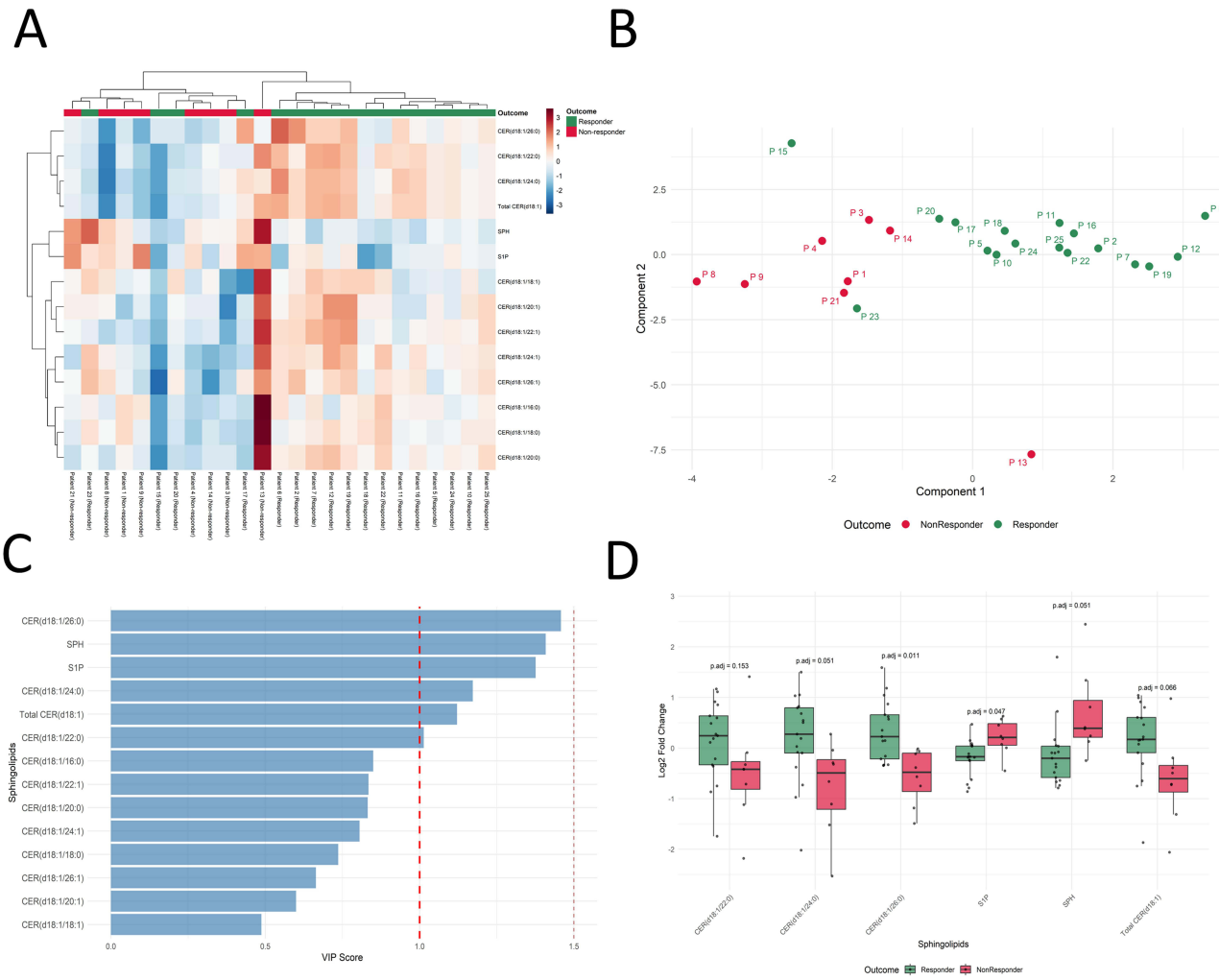

Figure 8 Dynamic remodeling of the plasma sphingolipid network following radiotherapy in a longitudinal sub-cohort (n=25). (**A**) Unsupervised hierarchical clustering heatmap of patients based on the fold changes (Log2FC) of all measured sphingolipids post-radiotherapy. The cluster annotation shows a significant association with clinical response (Fisher's exact test, p < 0.01). (**B**) Partial least squares-discriminant analysis (PLS-DA) score plot showing separation between responders (n=17) and non-responders (n=8) based on their post-radiotherapy sphingolipid fold-change profiles. (**C**) Variable Importance in Projection (VIP) scores from the PLS-DA model. The red vertical dotted lines indicate VIP scores of 1.0 and 1.5, respectively. The six sphingolipid species with VIP > 1.0 are shown, with CER(d18:1/26:0), SPH, and S1P being the top contributors. (**D**) Comparison of post-radiotherapy fold changes (Log2FC) for the sphingolipids with VIP scores>1 between responders and non-responders. Data are presented as median with interquartile range. Significant differences between groups after FDR adjustment are indicated by the exact P.adj values on the figure.

https://doi.org/10.2147/JHC.S580242

of the "sphingolipid rheostat" theory: in responders, the pro-survival sphingolipid S1P was significantly downregulated, SPH showed a decreasing trend, while pro-apoptotic ceramides were generally upregulated, with CER(d18:1/26:0) showing a significantly greater increase compared to non-responders (Figure 8D; detailed statistical data in Supplementary Table 15).

Discussion

This prospective lipidomics study provides preliminary evidence linking the plasma sphingolipid metabolic network to radiosensitivity in HCC. We demonstrated that incorporating key sphingolipid species, such as S1P and CER(d18:1/20:0), into a predictive model significantly enhanced its discriminatory performance (bootstrap-corrected AUC = 0.930), substantially outperforming the model based on conventional clinical parameters alone (AUC = 0.712). This marked improvement in predictive efficacy suggests that intrinsic tumoral sphingolipid metabolic reprogramming may represent a mechanism of radioresistance independent of traditional liver function and AFP status. This finding is consistent with the consensus from Preclinical studies that sphingolipid metabolism, as a master regulator of cell fate, plays a pivotal role in mediating radiation resistance when dysregulated.[6,20] Specifically, radiotherapy can promote the generation of pro-apoptotic ceramides by activating key enzymes including ceramide synthases (CerS) and acid sphingomyelinase (ASMase), while concurrently reducing pro-survival S1P levels by inhibiting sphingosine kinase 1 (SPHK1) or activating S1P lyase (SGPL1), thereby collectively driving the apoptotic program.[17] Our clinical data are consistent with the relevance of this regulatory network to the biological effects of radiotherapy in vivo.

The classical "sphingolipid rheostat" theory posits that cell fate is determined by the dynamic balance between pro-apoptotic ceramides and pro-survival S1P.[21] Our study provides preliminary clinical support for this concept. The CER/S1P ratio model constructed based on this concept demonstrated good overall discriminatory performance (bootstrap-corrected AUC = 0.828). More critically, analysis of covariance revealed that multiple CER/S1P ratios retained independent predictive value after controlling for the absolute concentration of S1P. This confirms that the metabolic balance state itself provides information beyond individual molecular concentrations and is also a determinant of radiotherapy response.

Notably, the two predictive models we developed offer distinct yet complementary insights into the biology of radiosensitivity. Model 1 (integrating S1P, CER(d18:1/20:0), ALP, and TBIL) demonstrates the potential value of incorporating plasma sphingolipids into a multivariate framework, achieving high discriminative accuracy in this cohort. In contrast, Model 2 (based on CER/S1P ratios and AFP) serves as a direct, clinically-informed validation of the "sphingolipid rheostat" theory, demonstrating that the balance between these opposing lipid species, rather than their absolute levels alone, is a key determinant of radiotherapy response in patients. The convergence of both models on the central role of sphingolipid metabolism provides compelling, multi-faceted support for its biological and clinical relevance in HCC radiosensitivity, establishing a strong rationale for future validation and mechanistic studies.

To capture the real-time metabolic response induced by radiotherapy, we performed a longitudinal dynamic analysis, extending the research perspective from static baselines to dynamic metabolic remodeling during treatment. The results revealed a coordinated, directional shift in the plasma sphingolipid profile of responders: pro-survival signaling (S1P) was significantly suppressed, while pro-apoptotic signaling—particularly CER(d18:1/26:0)—was strongly induced, exhibiting synchronous yet opposite dynamic patterns. This characteristic metabolic shift illustrates, at a systems level, how successful radiotherapy reprograms sphingolipid metabolism to push tumor cell fate towards the execution of apoptosis. This result lends support to the core hypothesis from preclinical studies: effective radiotherapy can shift the "sphingolipid rheostat" towards apoptosis.[20,22]

Notably, a recent study in colorectal cancer patients reported elevated levels of CER(d18:1/26:0) in tumor tissues, serum, and stool samples, which positively correlated with clinical indicators of tumor progression.[23] This finding appears to contradict our observation, to contradict our observation that increased plasma CER(d18:1/26:0) levels post-radiotherapy were associated with favorable treatment response. We posit that effective radiotherapy robustly activates key enzymes such as CerS within tumor cells, triggering large-scale apoptotic programs. Consequently, the observed rise in plasma CER(d18:1/26:0) levels is likely a consequence of radiotherapy-induced apoptosis—a direct biomarker reflecting extensive apoptotic death of tumor cells—rather than an indication of its intrinsic pro-proliferative role in

tumor progression. This interpretation aligns perfectly with the sphingolipid rheostat theory, wherein successful radiotherapy shifts the metabolic "balance switch" towards the pro-apoptotic end characterized by ceramide accumulation.

The immediate clinical value of our predictive model lies in its capacity to guide personalized therapeutic strategies at an early stage. Our model, which stratifies patients based on their probability of treatment response either prior to or shortly after radiotherapy, addresses a pressing unmet clinical need. Among the cohort, over 50% of patients were identified as potential responders—consistent with an objective response rate (ORR) of 54.1%—enabling clinicians to pursue radiotherapy within a multimodal treatment framework with enhanced confidence. More notably, the early identification of predicted non-responders facilitates a paradigm of "early triage," thereby avoiding continued exposure to the toxicities of an ineffective local treatment and allowing timely transition to alternative options, such as second-line systemic agents or clinical trial enrollment, while tumor burden remains more amenable to intervention. Moreover, in an evolving treatment landscape where radiotherapy is increasingly integrated with immunotherapy, our sphingolipid profile may provide a rational basis for patient selection, optimizing the use of such combination strategies.

In the current era of HCC management, which is increasingly centered on systemic therapy and emphasizes the synergy between local and systemic treatments, the role of radiotherapy is evolving from mere local ablation to an "immune-sensitizing" modality capable of modulating the tumor microenvironment (TME).[24] However, a major clinical challenge remains converting "cold" HCC tumors into immunotherapy-sensitive "hot" tumors and precisely identifying the patient subgroups most likely to benefit from combined radiotherapy-immunotherapy strategies.[25] Our findings offer a novel perspective on this challenge. The dynamic changes in the plasma sphingolipid profile we identified may have biological significance extending beyond regulating tumor cell fate to broadly influencing the TME, particularly anti-tumor immune responses. Our data show that radiotherapy response was accompanied by a significant decrease in circulating S1P levels. Importantly, recent studies have confirmed that baseline plasma S1P levels are significantly higher in HCC patients with poor response to immunotherapy compared to immunotherapy responders and have established that within the TME, S1P is primarily synthesized by tumor-associated macrophages (TAMs) and drives CD8+ T cell exhaustion via the S1P-S1PR1 axis.[11] To explore the implications of the S1P decrease observed in our cohort, one interpretation is that the observed decrease in S1P may directly promote tumor cell apoptosis. Furthermore, we speculate that this reduction could reflect broader alterations in the TME. Specifically, based on the established role of TAM-derived S1P in immunosuppression, it is plausible to hypothesize that a decrease in S1P might be associated with a shift towards a less immunosuppressive microenvironment. This hypothesis, however, requires direct validation in future studies. Building on this rationale, we hypothesize that the plasma sphingolipid profile—particularly the dynamic changes in S1P—could be explored as a potential biomarker for combining radiotherapy with immune checkpoint inhibitors. This easily accessible liquid biomarker might hold promise for prospectively identifying patients whose immunosuppressive TME has been successfully modulated, potentially making them more likely to benefit from combined strategies, thereby providing a candidate basis for personalized decision-making.

Sphingolipid metabolic intervention presents a highly promising dual-benefit strategy for synergistically enhancing radiotherapy efficacy. Numerous preclinical studies suggest that targeted modulation of sphingolipid metabolism holds potential for selectively sensitizing tumors while protecting normal tissues. On one hand, administering S1P or anti-ceramide antibodies in normal tissues can significantly mitigate radiation-induced damage to organs such as the ovaries,[26] gastrointestinal tract,[27] salivary glands,[28] and kidneys.[29] On the other hand, in tumor treatment, utilizing SPHK inhibitors (eg, FTY720),[30] CerS activators (eg, TPA),[31] or glucosylceramide synthase (GCS) inhibitors[32] can shift the sphingolipid balance towards pro-apoptotic ceramides, thereby reversing tumor radioresistance. Encouragingly, preliminary research introduces the concept of "therapeutic target reordering"—where the hierarchical susceptibility of different cell death pathways within a tissue can be therapeutically altered. This raises the intriguing possibility that by using sphingolipid-targeted therapies to inhibit the ASMase-mediated apoptotic pathway in normal tissues (eg, microvascular endothelium), the dominant mechanism of radiation injury could be therapeutically reordered. We hypothesize that this might, in turn, preferentially sensitize tumor cells to CerS-mediated apoptosis, thereby theoretically achieving a therapeutic window that protects normal tissues while enhancing tumor cell kill.[33] Therefore, a key focus of future research lies in exploring specific sphingolipid targets and drug delivery strategies capable of achieving this differential effect, ultimately advancing HCC radiotherapy into an era of high-efficacy and low-toxicity precision.

Limitation

This study establishes, for the first time, a clinical link between the plasma sphingolipid profile and radiosensitivity in HCC. However, several limitations must be acknowledged. First, as a single-center exploratory investigation, its sample size is modest, which is common in pioneering biomarker research where prior data for power calculations are unavailable. Consequently, all findings should be interpreted as hypothesis-generating. To ensure robustness within this constraint, we employed a rigorous statistical strategy: parsimonious model building, bootstrap internal validation and comprehensive performance assessment. Additionally, in the univariable screening phase, we used nominal p-values without multiplicity adjustment to maximize sensitivity for biomarker discovery, acknowledging the increased risk of Type I error. However, the key sphingolipid predictor (S1P) remained significant even after post-hoc FDR correction (Supplementary Table 16), and the subsequent multivariate modeling and validation steps further mitigated this risk. Therefore, while the observed discriminatory performance (AUC > 0.9) is promising and robustly signals a strong biological association, it does not represent a definitive clinical cutoff and requires confirmation in larger, multi-center, prospective cohorts. Second, while the use of plasma lipidomics offers the distinct advantage of being non-invasive, it may not fully capture the intricacies of the local sphingolipid metabolism within the tumor tissue itself. Future studies incorporating paired tumor samples for spatial lipidomic analysis would be invaluable in clarifying the cellular origins and functional roles of these sphingolipids within the tumor microenvironment. Third, this study excluded patients with severe metabolic disorders and, upon review, none of the enrolled patients were on medications known to significantly perturb systemic sphingolipid metabolism (eg, statins or corticosteroids). While this strengthens the internal validity of our findings by minimizing a key confounder, it also means that the predictive performance of the identified sphingolipid biomarkers remains to be validated in broader patient populations who may be using such medications.

Building upon these findings and acknowledging these limitations, future research should proceed along three principal directions: First, the clinical translation and validation of this model within a multi-center framework are essential to advance these sphingolipid markers into practical diagnostic tools. Second, employing preclinical models, such as patient-derived organoids or orthotopic models, could elucidate the molecular mechanisms by which key sphingolipid species regulate radiosensitivity and identify novel, actionable therapeutic targets. Third, there is a compelling need to explore combination strategies that integrate sphingolipid metabolic modulators (eg, SPHK1 inhibitors, ASMase agonists) with radiotherapy, evaluating their synergistic antitumor efficacy and translational potential. These concerted efforts are crucial for ultimately advancing HCC radiotherapy into an era of high-precision treatment characterized by enhanced efficacy and reduced toxicity.

Conclusion

In conclusion, this study provides the first compelling preliminary clinical evidence that the plasma sphingolipid profile serves not only as a reliable, non-invasive predictive biomarker but also as a crucial window into the intrinsic metabolic state and stress response of tumors. Our work not only validates the relevance of the "sphingolipid rheostat" theory in the clinical radiotherapy setting but, more importantly, establishes a vital methodological foundation and preliminary rationale for future large-scale, sphingolipid-guided precision radiotherapy trials in HCC. It also provides initial clinical data support for developing such strategies, opening new avenues for metabolic intervention research aimed at overcoming radioresistance in liver cancer.

Abbreviations

HCC, Hepatocellular carcinoma; AFP, Alpha-fetoprotein; ALP, Alkaline phosphatase; TBIL, Total bilirubin; AUC, area under the curve; Cer, Ceramide; S1P, Sphingosine-1-phosphate; DCA, Decision curve analysis; FDR, False discovery rate; LC-MS/MS, Liquid chromatography-tandem mass spectrometry; mRECIST, modified Response Evaluation Criteria in Solid Tumors; OR, Odds ratio; ORR, Objective response rate; SBRT, Stereotactic body radiation therapy.

Data Sharing Statement

The datasets generated during and analyzed during the current study are available from the last corresponding author, Yiyi Li (Department of Radiation Oncology, Nanfang Hospital, Southern Medical University, Guangzhou, Guangdong, People's Republic of China; Email: liyiyi56@smu.edu.cn), upon reasonable request.

Ethics Approval and Consent to Participate

This prospective study was conducted in accordance with the Declaration of Helsinki and was approved by the Medical Ethics Committee of Nanfang Hospital, Southern Medical University (Approval No. NFEC-202407-K29). The study was registered on ClinicalTrials.gov (NCT06864221). All enrolled patients provided written informed consent.

Acknowledgments

We extend our gratitude to all the patients who participated in this study. We also thank the clinical and research teams at Nanfang Hospital for their support in patient recruitment, sample collection, and data management.

Author Contributions

All authors made a significant contribution to the work reported, whether that is in the conception, study design, execution, acquisition of data, analysis and interpretation, or in all these areas; took part in drafting, revising or critically reviewing the article; gave final approval of the version to be published; have agreed on the journal to which the article has been submitted; and agree to be accountable for all aspects of the work.

Funding

This research was funded by Basic and Applied Basic Research Foundation of Guangdong Province (2023A151503004, 2024A1515013204 and 2024A1515220089); Foundation of President of Nanfang Hospital, Southern Medical University (2023A011).

Disclosure

The authors report no conflicts of interest in this work.

References

1. Bray F, Laversanne M, Sung H, et al. Global cancer statistics 2022: GLOBOCAN estimates of incidence and mortality worldwide for 36 cancers in 185 countries. *Ca a Cancer J Clinicians*. 2024;74(3):229–263. doi:10.3322/caac.21834
2. Zhang J, Xu W, Lu W, et al. Advances and prospects of stereotactic radiosurgery and stereotactic ablative body radiotherapy: evolving paradigms in precision oncology. *Med Res*. 2025. doi:10.1002/mdr2.70051
3. European Association for the Study of the Liver. EASL clinical practice guidelines on the management of hepatocellular carcinoma. *J Hepatol*. 2025;82(2):315–374. doi:10.1016/j.jhep.2024.08.028
4. Zhong CR, Wu ZF, Zheng ZQ, et al. Radiotherapy-induced TACC3 confers resistance of HCC to radiotherapy and enhances IL4-dependent immunosuppression to exacerbate hepatocarcinogenesis. *Cancer Lett*. 2025;627:217819. doi:10.1016/j.canlet.2025.217819
5. Wu Y, Song Y, Wang R, Wang T. Molecular mechanisms of tumor resistance to radiotherapy. *Mol Cancer*. 2023;22(1):96. doi:10.1186/s12943-023-01801-2
6. Hannun YA, Obeid LM. Sphingolipids and their metabolism in physiology and disease. *Nat Rev Mol Cell Biol*. 2018;19(3):175–191. doi:10.1038/nrm.2017.107
7. Morad SA, Cabot MC. Ceramide-orchestrated signalling in cancer cells. *Nat Rev Cancer*. 2013;13(1):51–65. doi:10.1038/nrc3398
8. Liu Q, Zhang X, Qi J, et al. Comprehensive profiling of lipid metabolic reprogramming expands precision medicine for HCC. *Hepatology*. 2025;81(4):1164–1180. doi:10.1097/hep.0000000000000962
9. Liu Y, Hong Z, Tan G, et al. NMR and LC/MS-based global metabolomics to identify serum biomarkers differentiating hepatocellular carcinoma from liver cirrhosis. *Int J Cancer*. 2014;135(3):658–668. doi:10.1002/ijc.28706
10. Grammatikos G, Schoell N, Ferreirós N, et al. Serum sphingolipidomic analyses reveal an upregulation of C16-ceramide and sphingosine-1-phosphate in hepatocellular carcinoma. *Oncotarget*. 2016;7(14):18095–18105. doi:10.18632/oncotarget.7741
11. Zhang X, Lao M, Sun K, et al. Sphingolipid synthesis in tumor-associated macrophages confers immunotherapy resistance in hepatocellular carcinoma. *Sci Adv*. 2025;11(21):eadv0558. doi:10.1126/sciadv.adv0558
12. Wolrab D, Jirásko R, Cífková E, et al. Lipidomic profiling of human serum enables detection of pancreatic cancer. *Nat Commun*. 2022;13(1):124. doi:10.1038/s41467-021-27765-9
13. Cattrini C, Manfredi M, Barboro P, et al. Untargeted lipidomics reveal association of elevated plasma C18 ceramide levels with reduced survival in metastatic castration-resistant prostate cancer patients. *Sci Rep*. 2023;13(1):17791. doi:10.1038/s41598-023-44157-9

14. Qu T, Zhang S, Yang S, Li S, Wang D. Utilizing serum metabolomics for assessing postoperative efficacy and monitoring recurrence in gastric cancer patients. *BMC Cancer*. 2024;24(1):27. doi:10.1186/s12885-023-11786-2
15. Corsetto PA, Zava S, Rizzo AM, Colombo I. The critical impact of sphingolipid metabolism in breast cancer progression and drug response. *Int J Mol Sci*. 2023;24(3):2107. doi:10.3390/ijms24032107
16. Machala M, Procházková J, Hofmanová J, et al. Colon cancer and perturbations of the sphingolipid metabolism. *Int J Mol Sci*. 2019;20(23):6051. doi:10.3390/ijms20236051
17. Yuan X, Liu H, Li C, et al. Molecular mechanism and research progress of sphingolipid metabolism in regulating radiation-induced apoptosis using pan-cancer analysis. *Curr Cancer Drug Targets*. 2025;25. doi:10.2174/0115680096330365250101074248
18. Marvaso G, Barone A, Amodio N, et al. Sphingosine analog fingolimod (FTY720) increases radiation sensitivity of human breast cancer cells in vitro. *Cancer Biol Ther*. 2014;15(6):797–805. doi:10.4161/cbt.28556
19. Liao L, Liu Z, Liu L, et al. Targeting the ceramidase ACER3 attenuates cholestasis in mice by mitigating bile acid overload via unsaturated ceramide-mediated LXRβ signaling transduction. *Nat Commun*. 2025;16(1):2112. doi:10.1038/s41467-025-57330-7
20. Kolesnick R, Fuks Z. Radiation and ceramide-induced apoptosis. *Oncogene*. 2003;22(37):5897–5906. doi:10.1038/sj.onc.1206702
21. Moro K, Nagahashi M, Gabriel E, Takabe K, Wakai T. Clinical application of ceramide in cancer treatment. *Breast Cancer*. 2019;26(4):407–415. doi:10.1007/s12282-019-00953-8
22. Park MA, Mitchell C, Zhang G, et al. Vorinostat and sorafenib increase CD95 activation in gastrointestinal tumor cells through a Ca(2+)-de novo ceramide-PP2A-reactive oxygen species-dependent signaling pathway. *Cancer Res*. 2010;70(15):6313–6324. doi:10.1158/0008-5472.Can-10-0999
23. Qu R, Zhang Y, Kim B, et al. Microbial riboflavin inhibits ceramide synthase 3 to lower ceramide (d18:1/26:0) and delay colorectal cancer progression. *Cell Metab*. 2025;37(9):1852–1869.e8. doi:10.1016/j.cmet.2025.06.002
24. Chiang CL, Lee FAS, Chan KSK, et al. Survival outcome analysis of stereotactic body radiotherapy and immunotherapy (SBRT-IO) versus SBRT-alone in unresectable hepatocellular carcinoma. *Liver Cancer*. 2024;13(3):265–276. doi:10.1159/000533425
25. Fucikova J, Kepp O, Kasikova L, et al. Detection of immunogenic cell death and its relevance for cancer therapy. *Cell Death Dis*. 2020;11 (11):1013. doi:10.1038/s41419-020-03221-2
26. Morita Y, Perez GI, Paris F, et al. Oocyte apoptosis is suppressed by disruption of the acid sphingomyelinase gene or by sphingosine-1-phosphate therapy. *Nature Med*. 2000;6(10):1109–1114. doi:10.1038/80442
27. Rotolo J, Stancevic B, Zhang J, et al. Anti-ceramide antibody prevents the radiation gastrointestinal syndrome in mice. *J Clin Invest*. 2012;122 (5):1786–1790. doi:10.1172/jci59920
28. Yang T, Zhao Q, Hu M, et al. Sphingosine-1-phosphate alleviates irradiation induced salivary gland hypofunction through preserving endothelial cells and resident macrophages. *Antioxidants*. 2022;11(10):2050. doi:10.3390/antiox11102050
29. Francis M, Ahmad A, Bodgi L, et al. SMPDL3b modulates radiation-induced DNA damage response in renal podocytes. *FASEB J*. 2022;36(10): e22545. doi:10.1096/fj.202100186RR
30. Pchejetski D, Bohler T, Brizuela L, et al. FTY720 (fingolimod) sensitizes prostate cancer cells to radiotherapy by inhibition of sphingosine kinase-1. *Cancer Res*. 2010;70(21):8651–8661. doi:10.1158/0008-5472.Can-10-1388
31. Garzotto M, Haimovitz-Friedman A, Liao WC, et al. Reversal of radiation resistance in LNCaP cells by targeting apoptosis through ceramide synthase. *Cancer Res*. 1999;59(20):5194–5201.
32. Iwasawa T, Zhang P, Ohkawa Y, et al. Enhancement of malignant properties of human glioma cells by ganglioside GD3/GD2. *Int J Oncol*. 2018;52 (4):1255–1266. doi:10.3892/ijo.2018.4266
33. Ch'ang HJ, Maj JG, Paris F, et al. ATM regulates target switching to escalating doses of radiation in the intestines. *Nature Med*. 2005;11 (5):484–490. doi:10.1038/nm1237